Processing Rusty Metals into Versatile Prussian Blue for Sustainable Energy Storage

Jian Peng
University of Wollongong
Wang Zhang
University of Wollongong
Jinsong Wang
Kunming University of Science and Technology
Lin Li
Nankai University https://orcid.org/0000-0002-4342-6816
Weihong Lai
University of Wollongong
Qiuran Yang
University of Wollongong
Bin-Wei Zhang
University of Wollongong https://orcid.org/0000-0002-7023-5986
Xiaoning Li
Institute for Superconducting and Electronic Materials, Univeristy of Wollongong
https://orcid.org/0000-0001-5991-0955
Yumeng Du
Institute for Superconducting and Electronic Materials, Univeristy of Wollongong
Hanwen Liu
University of Wollongong
Jianli Wang
University of Wollongong https://orcid.org/0000-0001-9254-1661
Zhenxiang Cheng
Institute for Superconducting & Electronic Materials, Australian Institute of Innovative Materials, University of Wollongong, Innovation Campus, Squires Way, North Wollongong, NSW 2500
https://orcid.org/0000-0003-4847-2907
Lizhen Wang
Zhengzhou University of Light Industry
Shiwen Wang
Zhengzhou University of Light Industry
Jiazhao Wang
University of Wollongong

Shulei Chou (shulei@uow.edu.au)
Australian Institute for Innovative Materials, Institute for Superconducting and Electronic Materials, University of Wollongong, Innovation Campus, Squires Way, North Wollongong, NSW 2522, Australia.
https://orcid.org/0000-0003-1155-6082
Huakun Liu
University of Wollongong https://orcid.org/0000-0002-0253-647X
Shi Xue Dou
University of Wollongong https://orcid.org/0000-0003-3824-7693

Article

Keywords: batteries, energy storage, catalysis

Posted Date: April 5th, 2021

DOI: https://doi.org/10.21203/rs.3.rs-361418/v1

Version of Record: A version of this preprint was published at Advanced Energy Materials on October 13th, 2021. See the published version at https://doi.org/10.1002/aenm.202102356.

Abstract

To reach a closed-loop material system and meet the urgent requirement of sustainable energy storage technologies, it is essential to incorporate efficient waste management into designing new energy storage materials. Here, we reported a “two birds with one stone” strategy to transform rusty iron products into Prussian blue as high-performance cathode materials and recover the rusty iron products to their original status. Owing to the high crystalline and Na^+ content, the rusty iron derived Prussian blue shows a high specific capacity of 145 mAh g^{-1} and excellent cycling stability over 3500 cycles. Through the *in situ* X-ray diffraction and *in situ* Raman spectra, it is found that the impressive ion storage capability and stability are greatly related to the suppressed structure distortion during the charge/discharge process. The ions migration mechanism and possibility as universal host of other kinds of ions are further illuminated by density functional theory calculations. This work provides a new strategy for recycling wasted materials into high value-added materials for sustainable battery systems, and is adaptable in the nanomedicine, catalysis, sensors, and gas storage applications.

Introduction

Battery technologies, with the most famous members of lead-acid and lithium-ion batteries (LIBs), have revolutionized the industries and our lifestyles over the past century.[1] Along with the scale applications of electric vehicles (EVs) and stationary energy storage systems (ESSs), the global battery market grows explosively in recent years and the whole shipment volume is expected to step from the era of GWh into TWh in the next few years.[2] However, considering most rechargeable batteries rely on critical mineral commodities such as lead, cobalt and nickel, there are tremendous issues that limit their sustainable development, including environmental pollution and health implications for people living during artisanal mining, as well as the anticipated rising prices of rare minerals.[3] Beyond that, the production of electrode materials usually involves smelting and high-temperature sintering, which are high energy consumption and low efficiency.[4, 5] To achieve sustainable development of the battery technologies, it is vital to discover low-cost, non-toxic and environment friendly element, such as iron, to replace the traditional Pb/Co/Ni redox centres in the electrode.[6, 7, 8] Meanwhile, developing more cost-efficient manufacturing process is of equal importance.

Iron, one of the most abundant and non-toxic 3d element, have been widely used in our daily life benefitting from the improved strength, versatility, cost-effectiveness, and heat resistance of iron metal products.[9] While enjoying the convenience of these products, human beings suffer from huge waste due to the inevitable rusting of iron products in the moist atmosphere, which is close to one-quarter of the total iron production per year.[7, 10] The recycling of iron scrap is widely carried out today, however, we are currently far away from an effective strategy towards a large amount of iron rust.[5] In principle, iron rust could be recycled via reducing and melting, but is not cost-efficient compared to the production of iron or steel products from iron ore.[11] Inspired from the redox-active nature of iron in the battery electrode (e.g., Fe in $LiFePO_4$ cathode for LIBs), if a large amount of iron rust could be converted into useful battery

products through an eco-friendly and facile way, we can close the loop in turning waste into wealth for a green and sustainable society.

Herein, as a proof-of-concept, we demonstrate a facile “two birds with one stone” method to process the rusty iron into Prussian blue cathode materials for sodium-ion batteries (SIBs), while recovering the wasted iron products to their original status. Due to the slow crystal growth rate in the acid environment, the as-prepared rusty-derived Prussian blue (R-PB) shows high crystalline and sodium-ion content. This R-PB cathode displayed excellent Na-storage properties even compared with the PBs synthesized by analytically pure chemicals, which could deliver a high specific capacity of 145 mAh g^{-1} at 0.1 C, excellent rate performance up to 10 C with a capacity of 97.8 mAh g^{-1}, and ultra-long cycle life over 3500 cycles at 5 C with the capacity retention of 70.3%. *In situ* X-Ray diffraction (XRD) and *in situ* Raman analysis further revealed the excellent reversibility of R-PB during sodium ion insertion and desertion. Density functional theoretical (DFT) calculation showed that the R-PB framework is capable for $Li^+/Na^+/K^+$ ion storage, demonstrating its versatility for battery electrode. This work provides an efficient strategy to recycle waste chemicals into battery electrodes, which is also applicable in other potential applications like nanomedicine, catalysis, sensors, gas storage, etc.

Results And Discussion

Rusty nails are chosen as the raw material because they are easily available (Figure S1). They possess unknown complexities in either compositions or phases, showing great difficulties in the purpose of recycling. In attempts to re-use the iron source in rusty nails, we carry out a simple method to circulate the non-soluble iron rust into soluble ferrous/ferric ions for preparing high-performance cathode materials. Figure 1 illustrates the sustainable synthesis procedure of processing rust iron metals into the Prussian blue for rechargeable alkali-ion batteries. As shown in the flow chart and Figure S1, the rusty nails are successfully getting back to their original bright nail by removing the rust. During this procedure, the rust is dissolved by the acid, forming ferrous or ferric ions, which are substantially utilized for preparing R-PB. This treatment put forward a new strategy of low-cost, strong feasibility and sustainability for the industrialized large-scale energy storage system, compared to conventional high-temperature sintering method for battery electrodes.

Figure 2a shows the Rietveld refined neutron diffraction pattern of R-PB and the diffraction peaks match well with the single Prussian blue phase. Table S1 and Figs. 2b-c exhibit the refinement results representing the crystal structure of R-PB shows cubic phase with a space group of *Fm-3m* and the lattice parameters of a = b = c = 10.3354 Å with the volume of V = 1104.032406 $Å^3$. A high-spin FeN_6 octahedral is bonding with a low-spin FeC_6 by the octahedral by the C≡N with the Na^+ occupied the positions of 8c and 24d in the 3-dimension open cubic structure.[12] Soft X-ray absorption near edge structure (XANES) spectroscopy (Fig. 2d) was carried out to measure the local structure and chemical environment. The Fe L-edge XANES spectra reveal two peaks that have originated from the electron transitions to anti-bonding π^* states and unoccupied e_g orbitals[13]. The Fourier transforming infrared spectrum (FT-IR) spectra of R-

PB shows sharp absorptions at 3472, 2075 and 1617 cm^{-1} which could be attributed to O-H, C≡N and H-O-H bonds, respectively.[14, 15] From comparing these with the spectra of the standard reference samples, the Fe cations are a mixture of Fe^{2+} and Fe^{3+}. Thermogravimetric analysis (TGA) was measured to test the content of absorbed water and interstitial water from room temperature to 500°C in Ar. The weight loss of R-PB is 1.7% and 22.4% before 150°C and 310°C, respectively, which is due to the water molecules adsorbed on the surface and the lattice water in the vacancies.[6] According to the obtained atomic occupation and TGA shown in Table S1 and Fig. 2f, the chemical formula for R-PB could be represented as $Na_{1.57}Fe[Fe(CN)_6]_{0.836}\cdot 3.91H_2O$. The high Na^+ content and low $[Fe(CN)_6]$ vacancies amount of R-PB could significantly enhance the initial coulombic efficiency and suppress the side-reaction as cathode for SIBs.[16, 17] The morphologies of the R-PB are shown in Fig. 2g, the blue powder sample has nanocubic shape with the particle size of 50–150 nm and the scanning transmission electron microscopy (STEM) shows that all elements are uniformly distributed in the particles. The STEM energy-dispersive X-ray spectroscopy line analysis (Figure S4) confirms that there is no impurity in the particles, demonstrating the feasibility from complex waste to pure PBs.

The electrochemical performance of the R-PB was tested between 2.0-4.2 V using metal sodium as counter electrode. The cyclic voltammetry (CV) curves (Fig. 3a) clearly show the well-defined and symmetric redox couples of Fe^{2+}/Fe^{3+} during the first five cycles. As we reported previously[12], the redox pairs near 3.0, 3.3 and 3.8 V are due to three different sodium-ion storage sites at 2c (Na1, interstitial), 3d (Na2, edge) and 3e (Na3, face) in the 3-dimension open structure of R-PB.[12] The high plateaus of 4.05 V are related to the side-reaction between the electrolyte and the electrode caused by the interstitial water as well as the formation of SEI film, while the charge and discharge curves become highly reversible after the first cycle. It is worth noticing that the 2c position contributes more than 60% of Na^+ storage sites and whole capacity while the other two positions contribute the high potential plateau. The first five charge/discharge curves of R-PB at the current density of 0.1 C (1C = 150 mA g^{-1}) are exhibited in Fig. 3b, and the first discharge specific capacity of 145 mAh g^{-1} can be obtained with initial Coulombic efficiency (ICE) of ~ 90%. The plateaus at 3.0, 3.3 and 3.8 V are related to the different Na^+ storage energy barriers and the irreversible plateaus above 4.0 V disappeared after the second cycle, which is consistent with the CV analysis. The rate performances of R-PB were carried at different current densities from 0.2 C-10 C (Fig. 3c), it is worth noting that the R-PB shows excellent fast charging performance with the discharge specific capacities of 111.8, 108.6, 103.5, 97.8 mAh g^{-1} at the rate of 0.5, 1, 2, 5 C. Even when the current density further increased to 10 C, which means the batteries could be fully charged/discharged within 6 mins, the capacity still maintain at 93.8 mAh g^{-1}, corresponding to a capacity retention of ~ 83.8%. The capacity could recover to its initial value when the current density returns. The long-term cycling stability of the R-PB was studied at the current densities of 1 C and 5 C after activated at 0.1 C for 5 cycles. The R-PB shows better cycling performance at a high current density of 5 C that the capacity maintains at 70.25 % even after 3500 cycles, corresponding to the capacity fading rate of only 0.85 % per 100 cycles and 5.96 % per 100 cycles at 1 C. Benefiting from a well-controlled co-precipitation process in the acid solution, the R-PB shows low-vacancy concentration and suppressed crystal water content, leading to

high ICE, enhanced cycle and rate performance[16]. Compared to previously reported iron-based PB synthesized by analytically pure chemicals as cathode materials for organic SIBs, the R-PB is one of the most competitive candidates regarding both rate performance and cycling stability[18, 19, 20].

To further investigate the structural evolution of the R-PB sample, *in situ* PXRD and *in situ* Raman spectra analyses were carried out during the charging and discharging process. Figure 4a shows the *in situ* PXRD patterns of R-PB during the first cycle at the current density of 25 mA g^{-1} between 2.0-4.2 V. The main strong reflections of the (200), (220), (400) and (420) planes of R-PB are selected and enlarged individually for further study. All of the peaks gradually shifted to higher angles during the charging process, while the intensity and the half-peak breadth at ~ 17.1 ° and 24.5 ° became larger during the charging progress, indicating the lattice shrink and the internal structural strain[21] caused by the extraction of Na^+. The peak shifts are ascribed to the phase transition from cubic to tetragonal during the Na^+ extraction process and a mixture of cubic and tetragonal phases was formed[22, 23]. The peaks at ~ 38.8° and 47.3° are well matched to the Al current collector, which remain unchanged during the whole charge and discharge process. During the discharge process, all peaks shifted towards lower degree, however, could not return to their initial positions after discharged to 2.0 V, indicating the irreversible structural evolution. The irreversible lattice shrink and expansion process might due to the side reactions between the electrolyte and R-PB, in which the lattice water reacted with Na^+ and formed the $[NaH_2O]^+$, consistent with the first charge/discharge cycle and our previous work[24, 25]. In consideration of the highly sensitivity of $(C{\equiv}N)^-$ vibration stretching mode to the oxidation state of the bonding iron, *in situ* Raman spectra was further employed to determine the sodium content and the valance state variation of the iron ions during the charge and discharge during the second cycle[16]. Starting from the fully charged state, only a strong peak at 2149 cm^{-1} and a weak peak at 2172 cm^{-1} were observed, which could be ascribed to the *v* (CN) bonding with $Fe^{2+/3+}$. During the discharge process, the main peak shifts to a low wavenumber, demonstrating that the Fe^{3+} (Na content = 0) has been reduced to Fe^{2+} (Na content = 2) during the sodium insertion process. During the charging process, the peaks shift in reverse toward high wave number and finally resume their original positions after fully charged, indicating that the Fe^{2+} has been oxidized to Fe^{3+} accompanied with the extraction of Na^+. The above results indicate that the structure change of R-PB is highly reversible during the sodium-ion insertion and extraction process after the first cycle activation, which further contributes to the impressive long cycle life of R-PB as cathode materials for SIBs.

DFT calculations were further performed to deeply understand the intrinsic properties of the crystal structure that are responsible for the outstanding performance. The Na^+ diffusion energy barriers along with the a, b, and c axes are only 0.41 eV, which means that material-PB possibly possesses fast three-dimensional pathways for Na^+ ion diffusion. The relatively low energy barriers can be ascribed to the NASICON-type structure where the sodium can be accessed expediently, which greatly contributes to the enhanced rate performance of SIBs. As shown in Fig. 4e, the charge interaction between Na^+ ions and the framework is negligible, which is in favor of Na^+ migration. Furthermore, the average voltage of Fe^- as

host for $Li^+/Na^+/K^+$ have been provided in Fig. 4f, one can see that with the increases of $Li^+/Na^+/K^+$ concentration, the average voltage exhibits a decreasing tendency, and the computational voltage traces the experimental well where K^+ possess the highest voltage platform, indicating R-PB could also be applied as cathode materials for LIBs and potassium-ion batteries. Considering another raw material, sodium ferrocyanide, could be prepared from the wasted sodium cyanide and iron salt, it is possible to synthesis R-PB fully based on wasted materials, offering a more sustainable choice for close-of-loop waste recycle.

Conclusion

In summary, we have developed a facile synthesis strategy to directly convert waste materials into a universal alkali metal ion host for high-performance rechargeable batteries. Owing to the intact crystal structure and negligible structural distortion during the Na^+ insertion/extraction process, the waste-derived R-PB exhibits a high Na storage capability of 145 mAh g^{-1} and unprecedented cycle stability with ~ 70.3 % capacity retention over 3500 cycles when applied as cathode materials for SIBs. The DFT calculation further validates the potential of R-PB as cathode materials for multi kinds of rechargeable batteries. The proof-of-concept work provides new routes for the recycling of wasted metal into high value-added products, which are of great importance to build a resource-sustainable environment and open a promising prospect for large-scale energy storage applications.

Declarations

Acknowledgments

This work is financially supported by Australian Research Council (ARC) Discovery Project (DP180101453). We also thank Dr. Tania Silver for critical reading of the manuscript.

References

1. Larcher D, Tarascon JM. Towards greener and more sustainable batteries for electrical energy storage. *Nat Chem* **7**, 19-29 (2015).
2. Dunn B, Kamath H, Tarascon JM. Electrical energy storage for the grid: a battery of choices. *Science* **334**, 928-935 (2011).
3. Zhu X*, et al.* $LiMnO_2$ cathode stabilized by interfacial orbital ordering for sustainable lithium-ion batteries. *Nature Sustainability*, 1-10 (2020).
4. Zhao LF*, et al.* Hard Carbon Anodes: Fundamental Understanding and Commercial Perspectives for Na-Ion Batteries beyond Li-Ion and K-Ion Counterparts. *Advanced Energy Materials* **11**, 2002704 (2020).
5. Reck BK, Graedel TE. Challenges in metal recycling. *Science* **337**, 690-695 (2012).

6. Xu Y*, et al.* Structure Distortion Induced Monoclinic Nickel Hexacyanoferrate as High-Performance Cathode for Na-Ion Batteries. *Advanced Energy Materials* **9**, 1803158 (2019).
7. Shooshtarian S, Maqsood T, Wong PSP, Yang RBJ, Khalfan M. Review of waste strategy documents in Australia: analysis of strategies for construction and demolition waste. *International Journal of Environmental Technology and Management* **23**, 1-21 (2020).
8. Fang C*, et al.* Routes to High Energy Cathodes of Sodium-Ion Batteries. *Advanced Energy Materials* **6**, 1501727 (2016).
9. Wang YX, Chou SL, Liu HK, Dou SX. Reduced graphene oxide with superior cycling stability and rate capability for sodium storage. *Carbon* **57**, 202-208 (2013).
10. Awasthi AK, Li JL. An overview of the potential of eco-friendly hybrid strategy for metal recycling from WEEE. *Resources, Conservation and Recycling* **126**, 228-239 (2017).
11. Izatt RM, Izatt SR, Bruening RL, Izatt NE, Moyer BA. Challenges to achievement of metal sustainability in our high-tech society. *Chemical Society Reviews* **43**, 2451-2475 (2014).
12. Wang WL*, et al.* Understanding rhombohedral iron hexacyanoferrate with three different sodium positions for high power and long stability sodium-ion battery. *Energy Storage Materials* **30**, 42-51 (2020).
13. Hocking RK, Wasinger EC, de Groot FM, Hodgson KO, Hedman B, Solomon EI. Fe L-edge XAS studies of $K_4[Fe(CN)_6]$ and $K_3[Fe(CN)_6]$: a direct probe of back-bonding. *J Am Chem Soc* **128**, 10442-10451 (2006).
14. Peng J*, et al.* A Dual-Insertion Type Sodium-Ion Full Cell Based on High-Quality Ternary-Metal Prussian Blue Analogs. *Advanced Energy Materials* **8**, 1702856 (2018).
15. Song J*, et al.* Removal of interstitial H_2O in hexacyanometallates for a superior cathode of a sodium-ion battery. *J Am Chem Soc* **137**, 2658-2664 (2015).
16. You Y, Wu XL, Yin YX, Guo YG. High-quality Prussian blue crystals as superior cathode materials for room-temperature sodium-ion batteries. *Energy & Environmental Science* **7**, 1643-1647 (2014).
17. Yin J*, et al.* In Situ Self-Assembly of Core-Shell Multimetal Prussian Blue Analogues for High-Performance Sodium-Ion Batteries. *ChemSusChem* **12**, 4786-4790 (2019).
18. Li WJ, Han C, Cheng G, Chou SL, Liu HK, Dou SX. Chemical Properties, Structural Properties, and Energy Storage Applications of Prussian Blue Analogues. *Small* **15**, e1900470 (2019).
19. Chen JS*, et al.* Prussian blue, its analogues and their derived materials for electrochemical energy storage and conversion. *Energy Storage Materials* **25**, 585-612 (2020).
20. Zhou A*, et al.* Hexacyanoferrate-Type Prussian Blue Analogs: Principles and Advances Toward High-Performance Sodium and Potassium Ion Batteries. *Advanced Energy Materials* **11**, 2000943 (2020).
21. Li WJ*, et al.* Stress Distortion Restraint to Boost the Sodium Ion Storage Performance of a Novel Binary Hexacyanoferrate. *Advanced Energy Materials* **10**, 1903006 (2020).
22. Shang Y*, et al.* Unconventional Mn Vacancies in Mn–Fe Prussian Blue Analogs: Suppressing Jahn-Teller Distortion for Ultrastable Sodium Storage. *Chem* **6**, 1804-1818 (2020).

23. Xu Y, *et al.* Crystallization-induced ultrafast Na-ion diffusion in nickel hexacyanoferrate for high-performance sodium-ion batteries. *Nano Energy* **67**, 104250 (2020).
24. Li WJ, *et al.* Facile Method To Synthesize Na-Enriched $Na_{1+X}FeFe(CN)_6$ Frameworks as Cathode with Superior Electrochemical Performance for Sodium-Ion Batteries. *Chemistry of Materials* **27**, 1997-2003 (2015).
25. Wang W, *et al.* Reversible structural evolution of sodium-rich rhombohedral Prussian blue for sodium-ion batteries. *Nat Commun* **11**, 1-9 (2020).

Figures

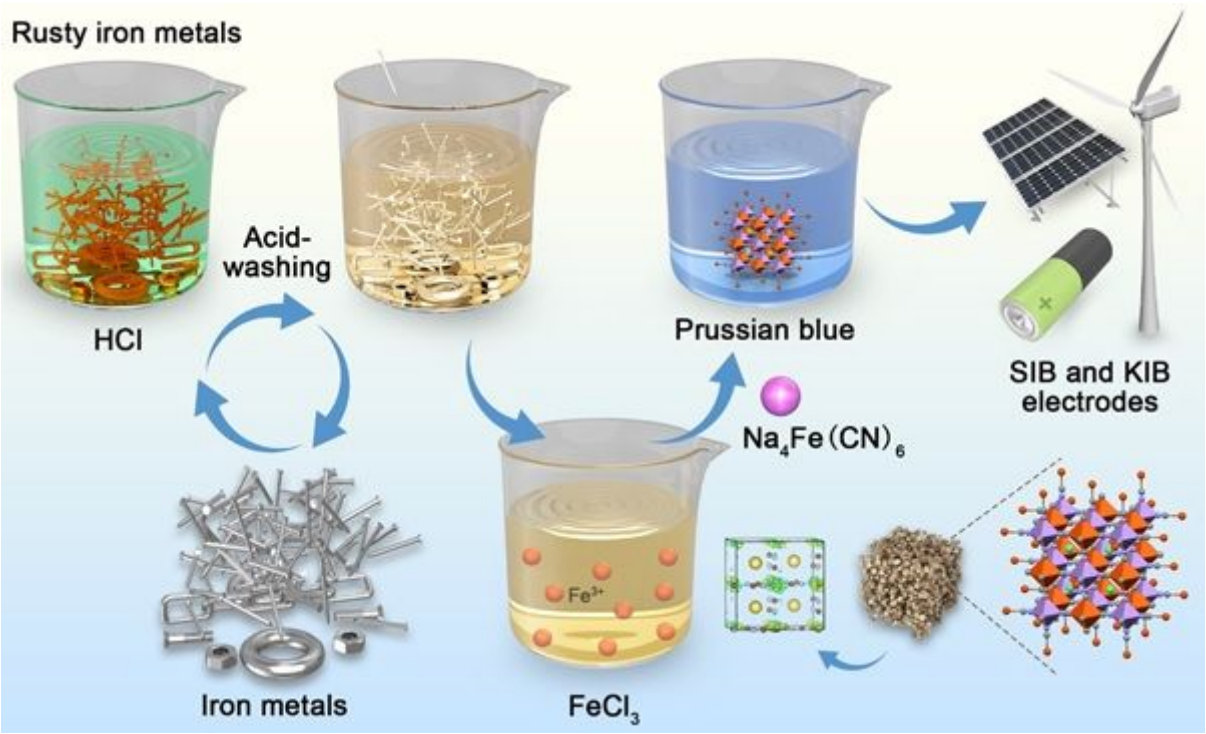

Figure 1

Illustration of processing scrap metals into versatile Prussian blue for alkali-ion (Li, Na, K) batteries.

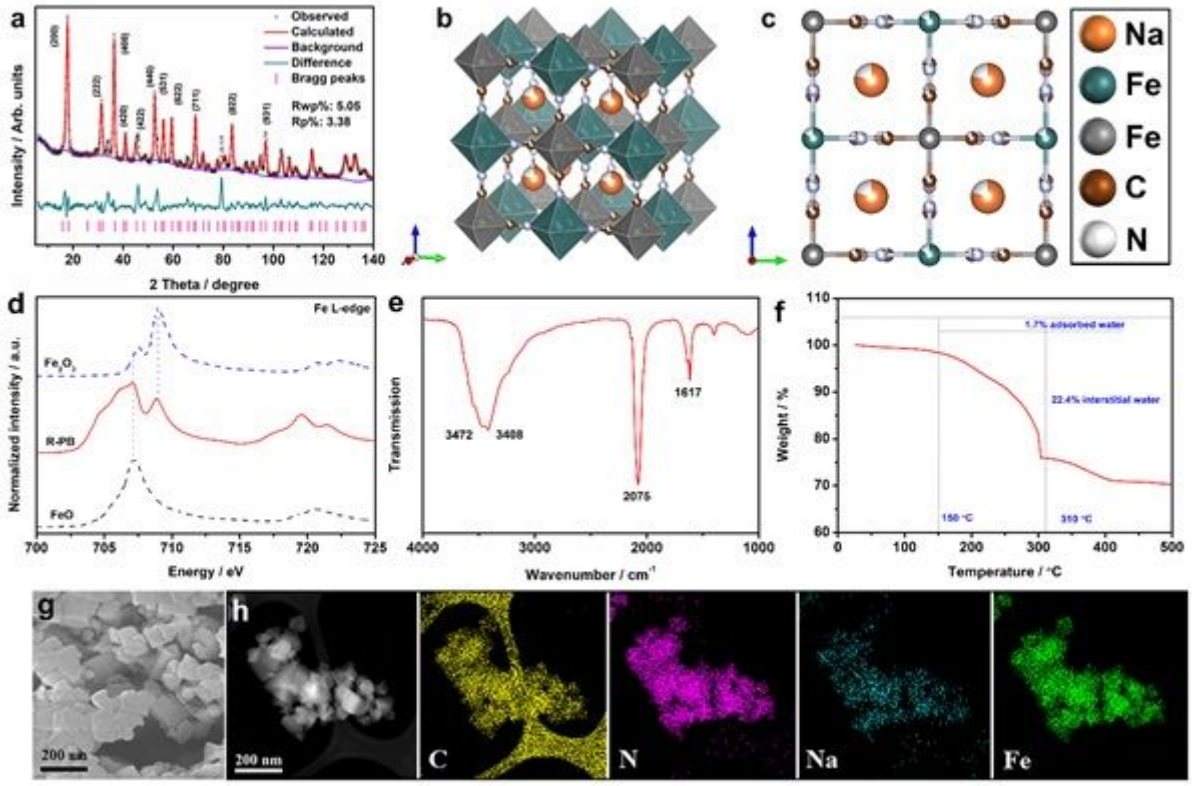

Figure 2

(a-c) Neutron powder diffraction Rietveld refinement pattern of R-PB and the corresponding lattice architecture of R-PB; (d) Fe L3-edge XANES spectra; (e) FTIR spectra; (f) TGA curves; (g) FESEM image and (h) STEM pattern and EDS elemental mapping of R-PB, including C, N, Na and Fe.

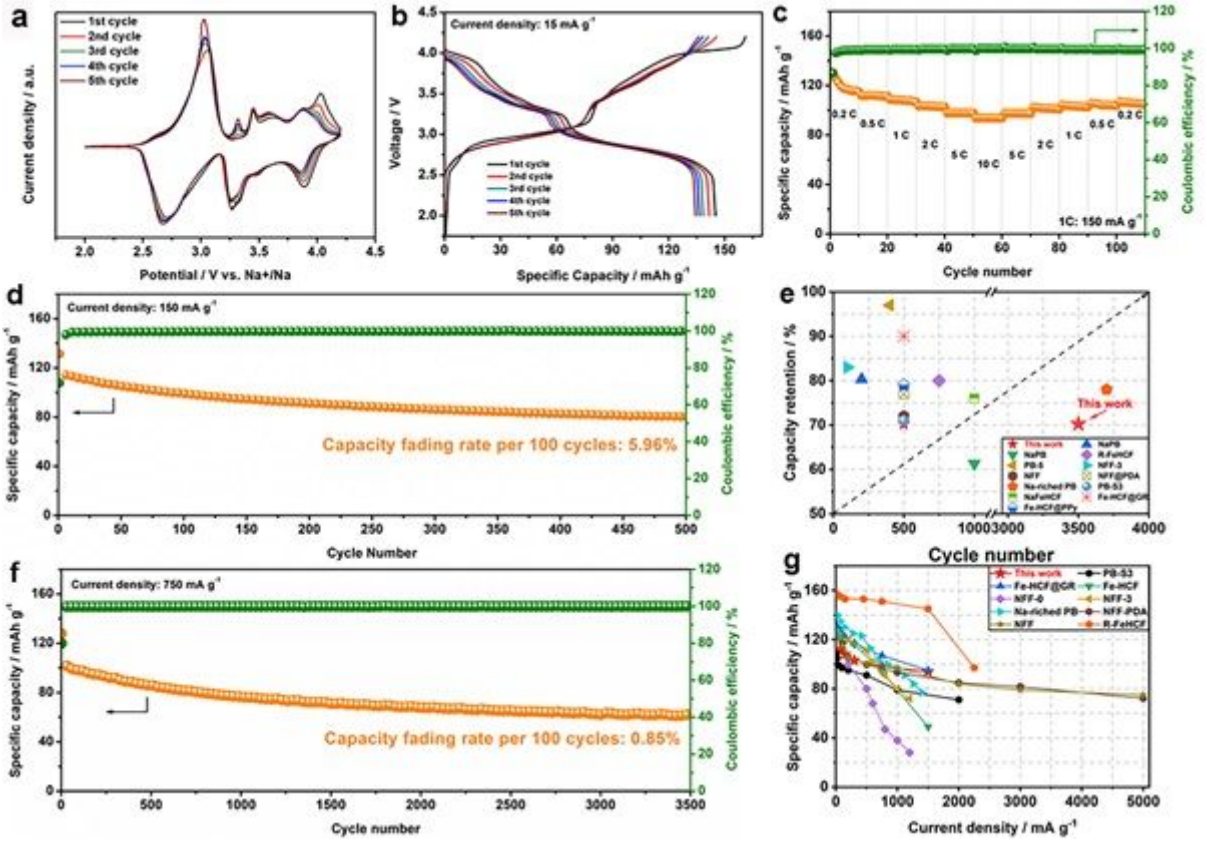

Figure 3

Electrochemical properties of the R-PB half cells for sodium-ion storage: (a) CV curves; (b) Charge-discharge curves at current density of 15 mA g-1; (c) Rate capabilities of R-PB at different current densities; (d) The long-life cyclability at current density of 150 mA g-1; (e) Cycle life and capacity retention comparison of various batteries; (f) The long-life cyclability at the current density of 750 mA g-1; (g) Rate performance comparison of various batteries.

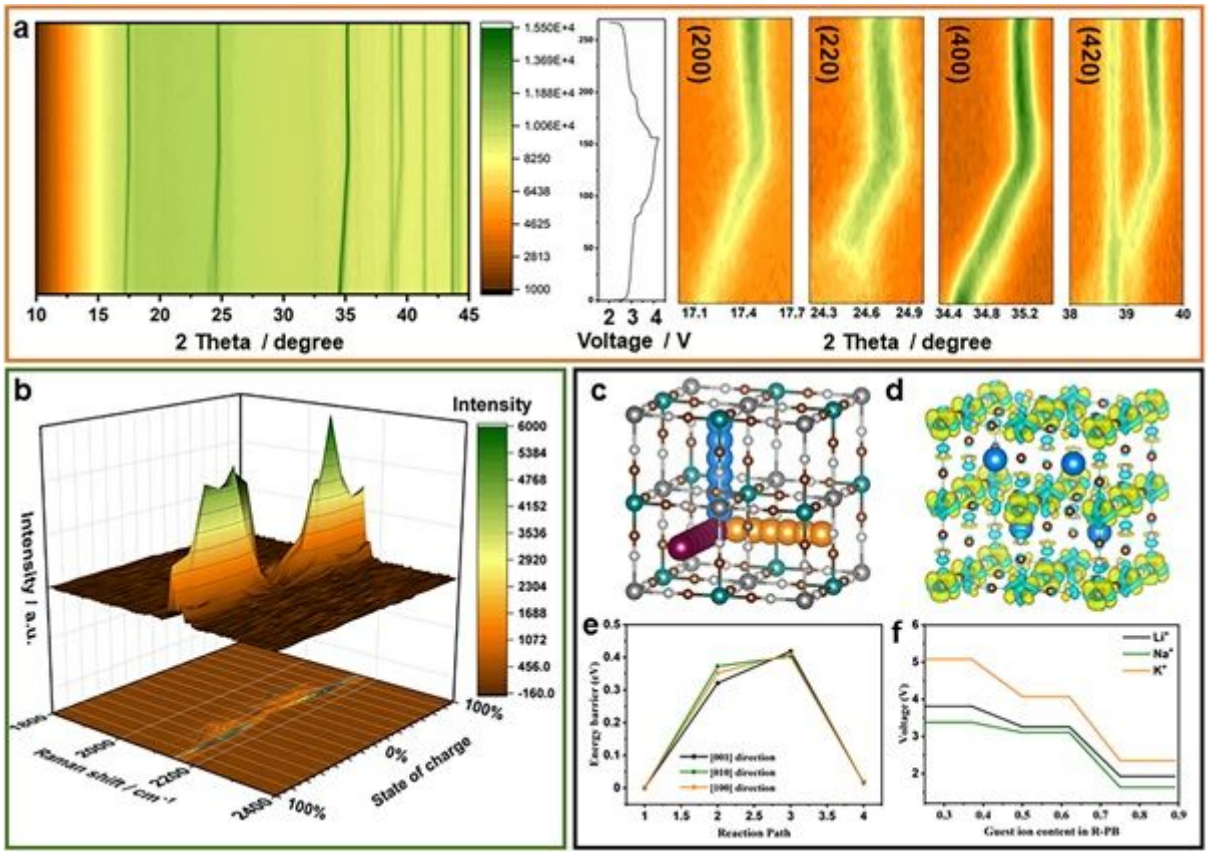

Figure 4

Alkali ion-storage mechanism investigations. (a) in situ PXRD patterns of R-PB with corresponding charge/discharge curves and 2D contour images of (200), (220), (400) and (420) peaks; (b) in situ Raman pattern during the second cycle; (c) representative Na+ migration paths within the open framework of R-PB; (d) Local charge density difference isosurfaces of Na embedded R-PB; (e) the migration activation energy of Na+ ion towards different directions within the crystal structure of R-PB; (f) average plateau of the R-PB as cathode materials for Li+/Na+/K+ batteries.

Supplementary Files

This is a list of supplementary files associated with this preprint. Click to download.

- Supportinginformation.docx